The Oscillatory Effects of Rhythmic Median Nerve Stimulation

Mairi S. Houlgreave[a,b], Barbara Morera Maiquez[a], Matthew J. Brookes[b], Stephen R. Jackson[a,c]

[a] *School of Psychology, University of Nottingham, University Park, Nottingham, NG7 2RD, UK*

[b] *Sir Peter Mansfield Imaging Centre, School of Physics and Astronomy, University of Nottingham, University Park, Nottingham, NG7 2RD, UK*

[c] *Institute of Mental Health, School of Medicine, University of Nottingham, University Park, Nottingham, NG7 2RD, UK*

Correspondence to:
Mairi Houlgreave, School of Psychology, University of Nottingham, University Park, Nottingham, NG7 2RD, UK.
E-mail address: mairi.houlgreave@nottingham.ac.uk (M.S. Houlgreave).

Abstract

Entrainment of brain oscillations can be achieved using rhythmic non-invasive brain stimulation, and stimulation of the motor cortex at a frequency associated with sensorimotor inhibition can impair motor responses. Despite the potential therapeutic applications, these techniques do not lend themselves to use outside a clinical setting. Here, the aim was to investigate whether rhythmic median nerve stimulation (MNS) could be used to entrain oscillations related to sensorimotor inhibition. MEG data were recorded from 20 participants during 400 trials, where for each trial 10 pulses of MNS were delivered either rhythmically or arrhythmically at 12 or 20Hz. Our results demonstrate a frequency specific increase in relative amplitude in the contralateral somatosensory cortex during rhythmic but not arrhythmic stimulation. This was coupled with an increase in inter-trial phase coherence at the same frequency, suggesting that the oscillations synchronised with the pulses of MNS. While the results show that 20Hz rhythmic peripheral nerve stimulation can produce entrainment, the response to 12Hz stimulation was largely due to the presence of rhythmic sensory evoked potentials. Regardless rhythmic MNS resulted in synchronous firing of neuronal populations within the contralateral somatosensory cortex meaning these neurons were *occupied* in processing of the afferent input. Therefore, MNS could prove therapeutically useful in disorders associated with hyperexcitability within the sensorimotor cortices.

Key Words

Magnetoencephalography; Median nerve stimulation; Mu; Beta; Entrainment; Steady-state evoked potentials

Highlights

- Rhythmic median nerve stimulation at 12Hz causes rhythmic sensory evoked potentials.
- Rhythmic median nerve stimulation at 20Hz causes entrainment of beta-band neural oscillations.

Abbreviations

AAL, Automated Anatomical Labelling; APB, abductor pollicis brevis; EMG, electromyography; FDR, false discovery rate; FLIRT, FMRIB's Linear Image Registration Tool; HT, Hilbert transform; ISI, inter-stimulus interval; ITPC, inter-trial phase coherence; LCMV, linear-constraint minimum-variance; MEPs, motor evoked potential; MNI, Montreal Neurological Institute; MNS, median nerve stimulation; NIBS, non-invasive brain stimulation; SAI, short afferent inhibition; SEP, sensory evoked potential; SMA, supplementary motor area; SSEP, steady-state evoked potential; tACS, transcranial alternating current stimulation; TFS, time frequency spectrogram; TMS, transcranial magnetic stimulation

1. Introduction

Neural oscillations are rhythmic variations in electrical activity which arise from the summation of synchronous postsynaptic potentials. Oscillations are categorised based on their frequency, with the alpha/mu (8-12Hz) and beta (13-30Hz) frequency bands being of particular importance when researching sensorimotor systems. In the contralateral sensorimotor cortex, oscillations in the 8-30Hz range are suppressed during movement and movement preparation, but following movement there is a beta rebound, meaning their amplitude is briefly higher than at rest (Jurkiewicz et al., 2006; Pfurtscheller et al., 1996). Corticospinal excitability is known to be increased when sensorimotor oscillations are suppressed and reduced during the post-movement beta rebound (Chen et al., 1998). Higher beta activity has also been associated with a slowing of newly initiated movements (Gilbertson, 2005). Therefore, beta synchrony is frequently thought of as a mechanism which promotes maintenance of the current motor set (Engel & Fries, 2010). However, a newer theory suggests that beta is a marker of motor readiness, whereby a low level of beta activity indicates a higher likelihood that a movement will be generated (N. Jenkinson & Brown, 2011). On the other hand, alpha (mu in the sensorimotor cortex) synchrony has been linked to the inhibition of task irrelevant areas (Brinkman et al., 2016; Jensen & Mazaheri, 2010), with the network of regions involved in a task showing a desynchronisation of alpha oscillations (Haegens et al., 2009). Various non-invasive brain stimulation (NIBS) techniques have been shown to modulate these oscillatory rhythms as well as behaviour (Pogosyan et al., 2009; Thut, Veniero, et al., 2011). As a result, there is widespread interest in the use of these techniques as potential forms of therapy in a multitude of disorders.

An interesting avenue for therapy using NIBS is entrainment; the process though which neuronal assemblies become synchronised to a rhythmic stimulus train (Thut, Schyns, et al., 2011). Entrainment of oscillations in the 8-30Hz range could prove therapeutically beneficial in patients with disorders characterised by sensorimotor hyperexcitability. Therefore, it is of interest that repetitive transcranial alternating current stimulation (tACS) at a frequency associated with periods of decreased corticospinal excitability can lead to a reduction in the velocity of movement (Pogosyan et al., 2009). In 2011, Thut and colleagues showed that rhythmic TMS stimulation of a parietal site at individual alpha frequency caused region specific entrainment of brain oscillations (Thut, Veniero, et al., 2011). These findings were specific to rhythmic TMS and were not seen with arrhythmic or sham stimulation (Thut, Veniero, et al., 2011). Given that tACS can have similar oscillatory effects it is interesting that application of a topical anaesthetic can significantly reduce entrainment, suggesting that the effects of tACS may be due to stimulation of the somatosensory cortex via peripheral nerves rather than direct stimulation of the cortex itself (Asamoah et al., 2019). This indicates that there is potential for the

same effect to be replicated through rhythmic stimulation of peripheral nerves rather than the cortex (Asamoah et al., 2019). In fact, rhythmic median nerve stimulation (MNS) at 12Hz and 19Hz (preprint) has shown similar entrainment effects in healthy participants, using sensor level EEG analysis (Maiquez et al., 2020; Morera Maiquez et al., 2020). Furthermore, concurrent delivery of 12Hz rhythmic MNS has been shown to slow reaction times compared to arrhythmic stimulation in a choice reaction time task (Morera Maiquez et al., 2020). These are important findings as, unlike tACS and TMS, MNS is portable, cheaper and requires little training, making it an ideal technique to be used therapeutically outside of the clinic.

When a sensory stimulus (such as MNS) is delivered a transient, phase-locked electrical potential can be recorded over the sensorimotor cortex which is known as a sensory evoked potential (SEP) (Vialatte et al., 2010). When longer trains of rhythmic stimuli are delivered, we can record steady-state evoked potentials (SSEPs) which appear as a sustained response at the frequency of stimulation (Regan,1989, as cited in (Vialatte et al., 2010)) (Regan, 1966). SSEPs are thought to either arise due to entrainment of a population of neurons (Herrmann, 2001) or due to linear superposition of SEPs in response to each pulse of the train (Capilla et al., 2011). Critically, both explanations could explain the increase in EEG/MEG power and inter-trial phase coherence (ITPC) at the frequency of stimulation (Capilla et al., 2011; Keitel et al., 2014). When refractoriness is taken into account there is compelling evidence for the superposition hypothesis (Capilla et al., 2011; Colon et al., 2012). Nevertheless, there is reason to believe both mechanisms coexist (Colon et al., 2012; Notbohm et al., 2016). Oscillating systems have a preferred frequency and when matched by the external stimulus train the system resonates (Colon et al., 2012; Herrmann, 2001; Notbohm et al., 2016; Vialatte et al., 2010). Therefore, at certain frequencies the signal recorded could be largely because of entrainment rather than rhythmic SEPs (Colon et al., 2012). Hence, in our study we delivered trains of MNS at 12 and 20Hz during concurrent MEG recording to investigate entrainment effects (adapted from (Morera Maiquez et al., 2020)). Replication of this experiment in MEG is important to ensure validity of the findings and to probe the effects in the somatosensory cortex. In MEG the signal is less affected by the conductivity of the overlying tissue compared to EEG (Cheyne, 2013), and therefore the models used for source localisation are simpler due to the lower level of spatial smearing (Muthukumaraswamy, 2014). Here we hypothesise there will be entrainment of oscillations within the contralateral somatosensory cortex during rhythmic, but not arrhythmic, MNS. To conclude that rhythmic MNS induces entrainment we will need to show (i) a frequency and region-specific increase in power, (ii) synchronisation of the phase with the external source and (iii) that these effects are not purely due to rhythmic evoked potentials.

2. Experimental Procedures

2.1. Subjects

Twenty healthy participants were recruited for the study. Nineteen participants were right handed according to the Edinburgh Handedness Inventory (Oldfield, 1971). Participants gave informed consent and the experimental paradigm received local ethics committee approval (School of Psychology, University of Nottingham). Participants agreed that pre-existing structural MRI data (obtained within the Sir Peter Mansfield Imaging Centre, University of Nottingham) could be used by the researchers. One participant (female, 21 years old, right-handed) was excluded prior to analysis due to excessive movement during the MEG recording, leaving 19 usable datasets (aged 26.7 ± 3.6 years (mean ± SD); 11 female)

2.2. Median Nerve Stimulation

Stimulation was delivered with electrodes (cathode proximal) positioned on the right forearm over the median nerve, using a Digitimer constant current stimulator model DS7A (Digitimer Ltd, UK). Pulse width was set at 0.2ms and Vmax at 400V. Participants were seated and told to rest their forearm on the chair armrest to ensure the muscles were relaxed. The stimulation threshold was set at the minimum intensity required for a visible thumb twitch (mean ± SD) 9.1 ± 3.2 mA.

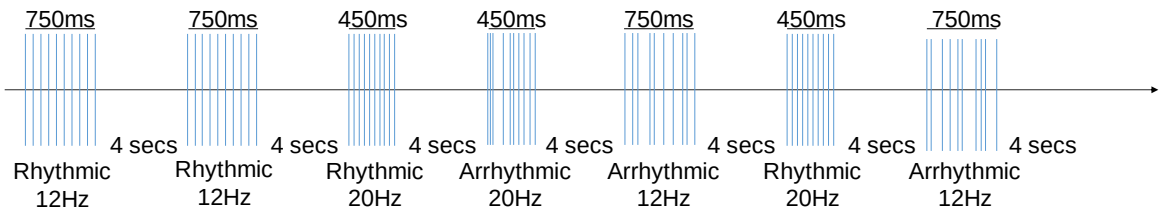

Figure 1. Stimulation overview.
A diagram showing an example of the trial setup for the MNS.

Four hundred trials of stimulation were delivered to the right median nerve during concurrent MEG recording, with a short break every 100 trials. Each trial consisted of 10 pulses delivered at the frequency of interest, rhythmic 12Hz and 20Hz in the test conditions. Arrhythmic controls were used to ensure that similar responses did not occur with random high frequency stimulation. During the control trials the same number of pulses were delivered as in the test condition, but with a random inter-stimulus interval (ISI) which was on average the same as the rhythmic trials (but constrained to a minimum ISI of 0.01s). The arrhythmic patterns were not the same for all trials or participants, however, the first pulse was always delivered at time 0 and the last pulse was always delivered at the

end of the train (450 or 750ms), regardless of the condition. For each of these 4 conditions, 100 trials were randomly delivered with an inter-trial interval of 4s using an in-house Matlab script (Matlab R2012a, Mathworks, Natick, MA) (Figure 1).

2.3. EMG Measurement

Electromyography (EMG) electrodes were placed over the right abductor pollicis brevis (APB) muscle in a belly tendon montage to allow motor evoked potentials (MEPs) to be recorded for twenty pulses of MNS at the intensity for a minimum thumb twitch, with 3s between each pulse. A Brainamp ExG (Brain Products GmbH, Gilching, Germany) was used to amplify the signal and Brain Vision Recorder (Brain Products GmbH, Gilching, Germany) was used to record the EMG data (bandpass filtered 10-2000Hz, sampling rate 5kHz). Peak-to-peak amplitudes were measured using an in-house Matlab script to determine the baseline MEP amplitude (mean = 1219.13µV, range = 52.10 - 7490.9µV) (Matlab R2017a, Mathworks, Natick, MA). EMG data from 6 individuals was not recorded due to technical issues.

2.4. MEG Data Acquisition

MEG data were collected at the Sir Peter Mansfield Imaging Centre, University of Nottingham using a 275-channel CTF MEG system (MISL, Coquitlam, Canada) with participants in a seated position. The system was operated in a third order synthetic gradiometer configuration and data sampled at 600Hz. Fiducial marker coils were placed on the nasion and bilateral preauricular points of the participants, to track head movement in relation to the MEG sensors. A Polhemus FASTRAK (Polhemus Inc, Vermont) was used to digitise the participants' head shape and the relative positions of the fiducial markers. The data was examined by eye using DataEditor (CTF MEG, Canada) and trials containing large artefacts were discarded, as were trials where the head moved more than 7mm from its initial position. This resulted in the removal of 8 rhythmic 12Hz, 9 arrhythmic 12Hz, 8 rhythmic 20Hz and 9 arrhythmic 20Hz trials on average per subject. The data were then segmented such that an epoch started 1s before stimulation and ended 3s following the end of stimulation. The epoch lengths of alpha and beta trials were 4.75s and 4.45s, respectively. An anatomical MRI scan (1.0mm^3 resolution, MPRAGE sequence) from each subject was used for co-registration to the digitised head shape.

2.5. Data Analysis

After pre-processing, a linear-constraint minimum-variance (LCMV) beamformer was applied to the data (Van Veen et al., 1997). Using FLIRT (FMRIB's Linear Image Registration Tool) (M. Jenkinson et al., 2012), a MNI (Montreal Neurological Institute) template brain was warped with respect to the

subject's downsampled (4mm) anatomical scan, as was the AAL (Automated Anatomical Labelling) atlas (Tzourio-Mazoyer et al., 2002). This allowed the cortex to be parcellated into 78 regions and the coordinates of the centroids from each region to be determined for each individual (Gong et al., 2009). Covariance was calculated for the entire experimental time window within a 1-150Hz frequency window (Brookes et al., 2008). The covariance matrix of the filtered data was regularised using the Tikhonov method, with the regularisation parameter set at 5% of the maximum singular value. The forward model was computed using dipole approximation and a multiple local spheres head model (Huang et al., 1999; Sarvas, 1987). Dipoles were rotated in the tangential plane to determine the orientation which yielded the maximum signal-to-noise ratio. Beamformer weights were calculated for the centroid of each brain region resulting in 78 timecourses (O'Neill et al., 2017), which were filtered between 1 and 48Hz. Symmetric orthogonalisation was implemented to ensure the timecourses from distinct regions were independent (Colclough et al., 2015).

2.6. Time Frequency Spectrograms

To visualise power changes across the trial, time frequency spectrograms (TFSs) were calculated. Data were filtered into frequency bands spanning from 4 to 50Hz, with a 50% overlap, to visualise the changes across frequency bands in the left somatosensory cortex as defined by the AAL atlas. The analytic signal for the data within each band was determined using a Hilbert transform (HT), the absolute value of which gave the power of the MEG signal at each point in time. Timecourses for each frequency band were then averaged across trials, before being normalised using the average power during the control window (0.24-0.99s for 12Hz trials and 0.54-0.99s for 20Hz trials). TFSs were averaged across subjects.

2.7. Inter-Trial Phase Coherence

The timeseries from the contralateral somatosensory cortex were filtered into the same frequency bands as were previously used for the TFSs calculation. Following a HT of the data, the ITPC was calculated using formula (1) below:

$$ITPC = \left| \frac{1}{N} \sum_{k=1}^{N} exp^{i * \emptyset k} \right| \quad (1)$$

Where N is the number of trials and Φk is the phase angle in radians of the datapoint in the current trial.

2.8. Statistical Analysis

For both the power and ITPC, timecourses were filtered according to the frequency of stimulation (11-13Hz or 19-21Hz) and were statistically compared using a one-tailed Wilcoxon signed rank test at each timepoint. Multiple comparisons were corrected for using the false discovery rate (FDR) of 0.05 (Benjamini & Hochberg, 1995; Benjamini & Yekutieli, 2001; Groppe, 2020). Post-hoc timecourse analysis was completed in the same manner but with a two-tailed test. All timecourse plots show the standard error of the mean (SEM) (Martínez-Cagigal, 2020).

3. Results

All analyses were conducted on the contralateral (left) *somatosensory* cortex as defined by the AAL atlas. Figures for similar analyses on the contralateral *motor* cortex are given in Appendix A.

3.1. Entrainment: Increase in Power

During the delivery of 10 rhythmic pulses at 12Hz, there was an increase in raw oscillatory amplitude at 12Hz (Figure 2A) within the contralateral sensorimotor cortex. This increase was not evident during arrhythmic stimulation where a decrease in amplitude was seen bilaterally in the sensorimotor cortices (Figure 2B). Similarly, during the 20Hz rhythmic condition there was an increase in the raw oscillatory amplitude at 20Hz (Figure 3A) within the contralateral sensorimotor cortex, which was not evident during arrhythmic stimulation at the same average frequency (Figure 3B). Interestingly, the ipsilateral sensorimotor cortex appeared to show a larger decrease in amplitude than the contralateral cortex during arrhythmic stimulation.

Evidence of rhythmic entrainment comes from the TFSs where there was an initial broadband increase in power associated with the first pulse (1s) of both rhythmic (Figure 4A, Figure 6A) and arrhythmic stimulation (Figure 4B, Figure 6B), which became specific to a narrowband around the frequency of stimulation during only rhythmic stimulation (Figure 4A, Figure 6A). This increase in MEG power returned to baseline shortly after the last pulse in the rhythmic condition. When the arrhythmic TFS is subtracted from the rhythmic TFS, it is evident that the difference between trials occurred only during the delivery of stimulation (Figure 4C, Figure 6C). The 12Hz power within the window of stimulation was significantly higher in the rhythmic condition compared to arrhythmic ($p \leq 0.05$ between 1162 and 1893ms, FDR corrected) (Figure 5A). Conversely, the 20Hz power increase within the window of stimulation in the rhythmic condition compared to arrhythmic did not survive FDR correction (Figure 7A). As the arrhythmic condition involved pulses being delivered at different times during every trial, power changes may have been averaged out during calculation of the TFS.

Therefore, the average power change for every trial during the delivery of MNS at 20Hz was calculated and then averaged across trials, showing a significantly higher 20Hz power in the rhythmic compared to the arrhythmic condition (t=172, z=3.10, p = 0.0019) (Figure 7B). Analysis of the average power across trials in the 12Hz condition again showed significantly higher 12Hz power in the rhythmic condition (t=189, z=3.78, p≤0.001) (Figure 5B).

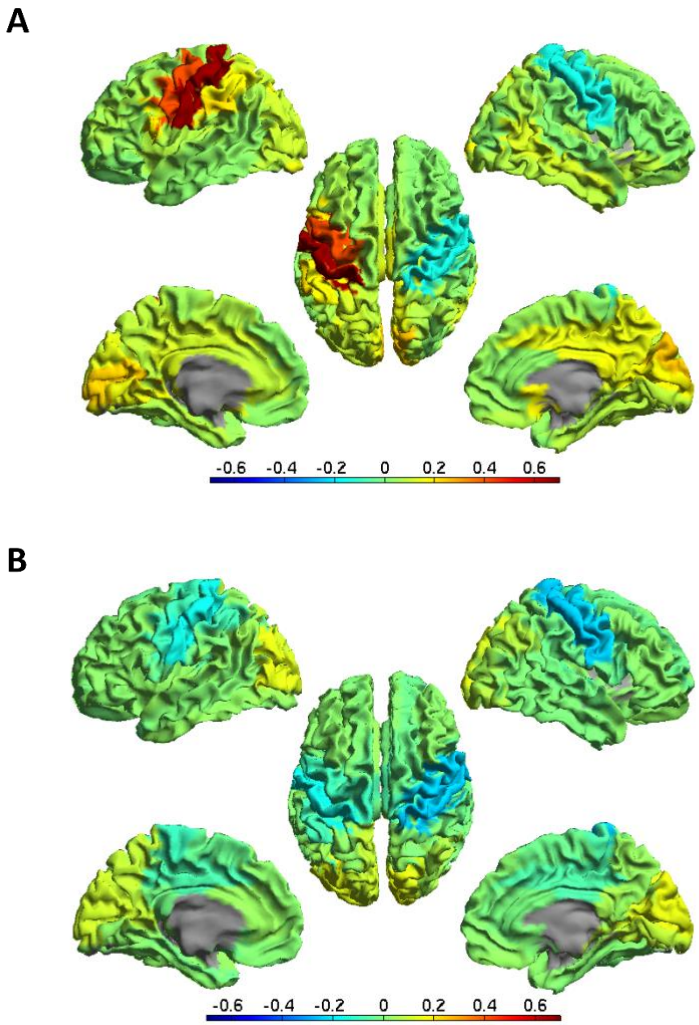

Figure 2. Localisation of the source of 12Hz oscillatory changes compared to baseline.
Raw 12Hz oscillatory amplitude for 78 cortical regions of the AAL atlas during A) rhythmic 12Hz MNS and B) arrhythmic 12Hz MNS.

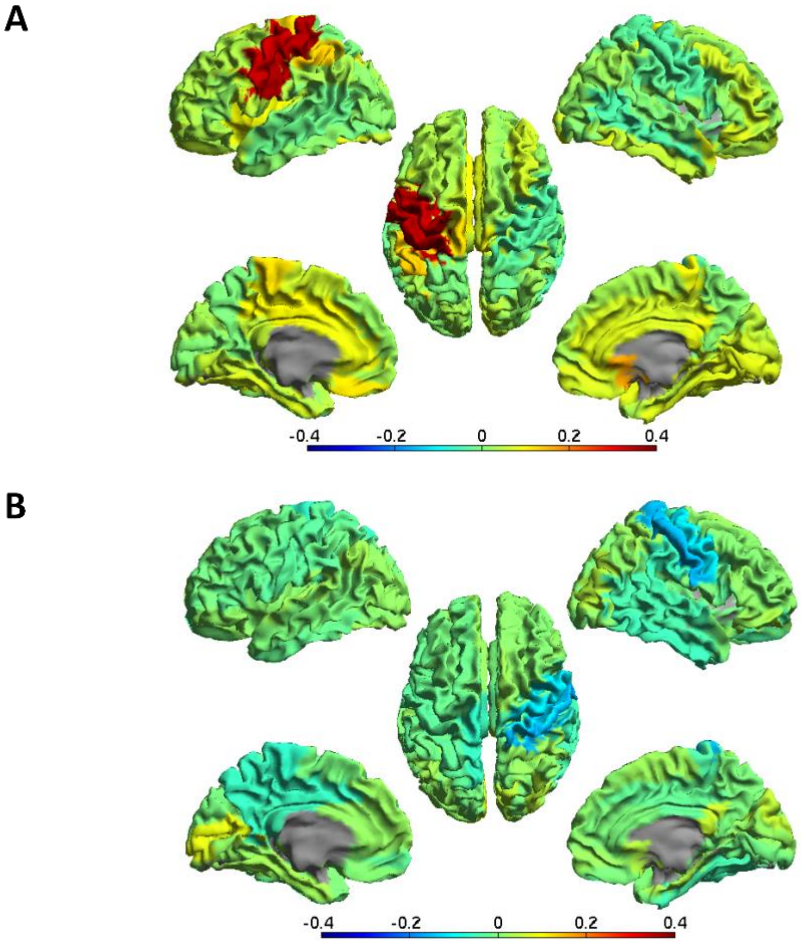

Figure 3. Localisation of the source of 20Hz oscillatory changes compared to baseline.
A figure showing the raw 20 Hz oscillatory amplitude for 78 cortical regions of the AAL atlas during A) rhythmic 20Hz MNS and B) arrhythmic 20Hz MNS.

1

1

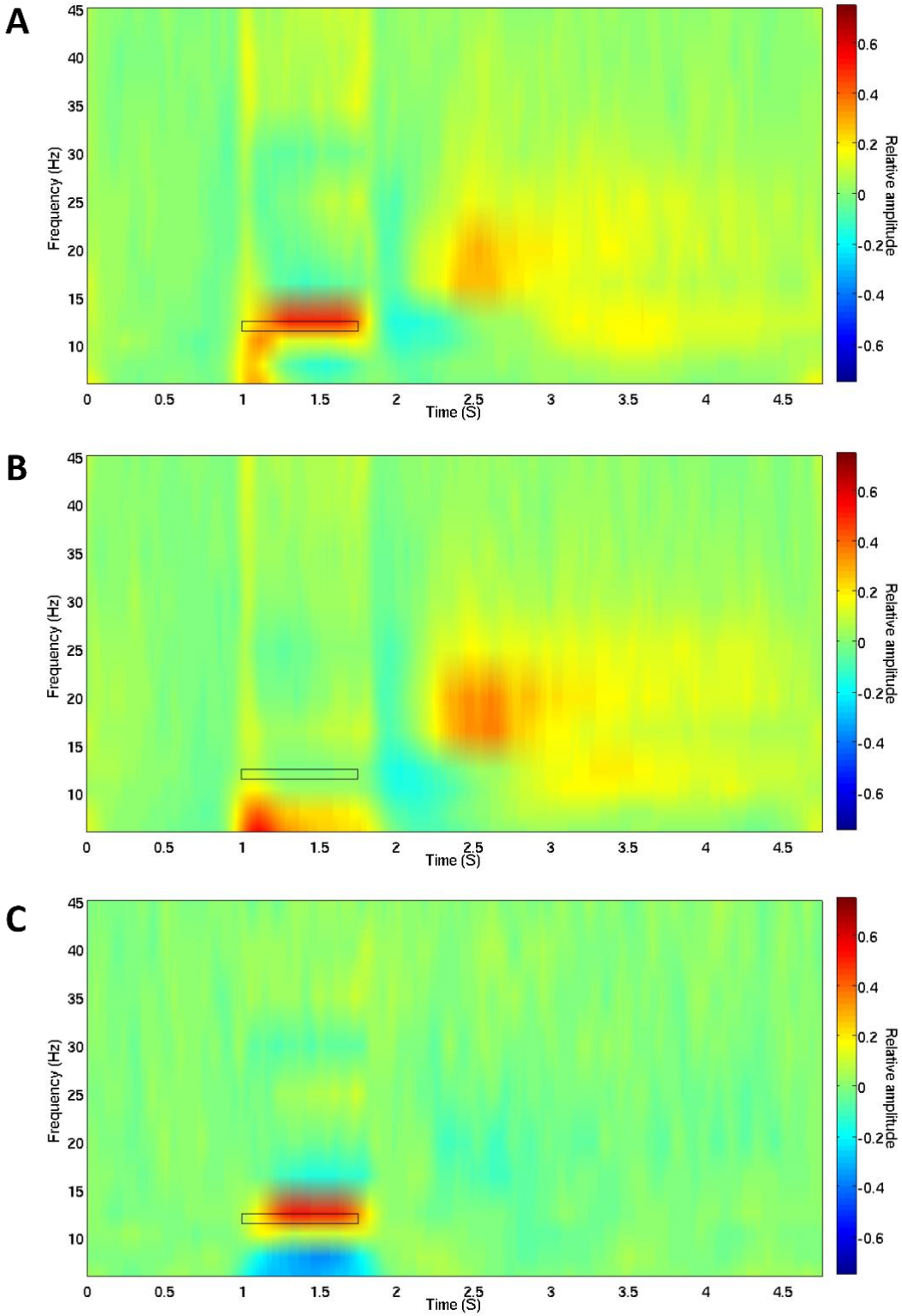

Figure 4. 12Hz power in the contralateral somatosensory cortex.

(A-C) TFSs of relative amplitude changes when 12Hz MNS was delivered between 1 and 1.75s in either a A) rhythmic or B) arrhythmic pattern with C) showing the difference in power between the two conditions.

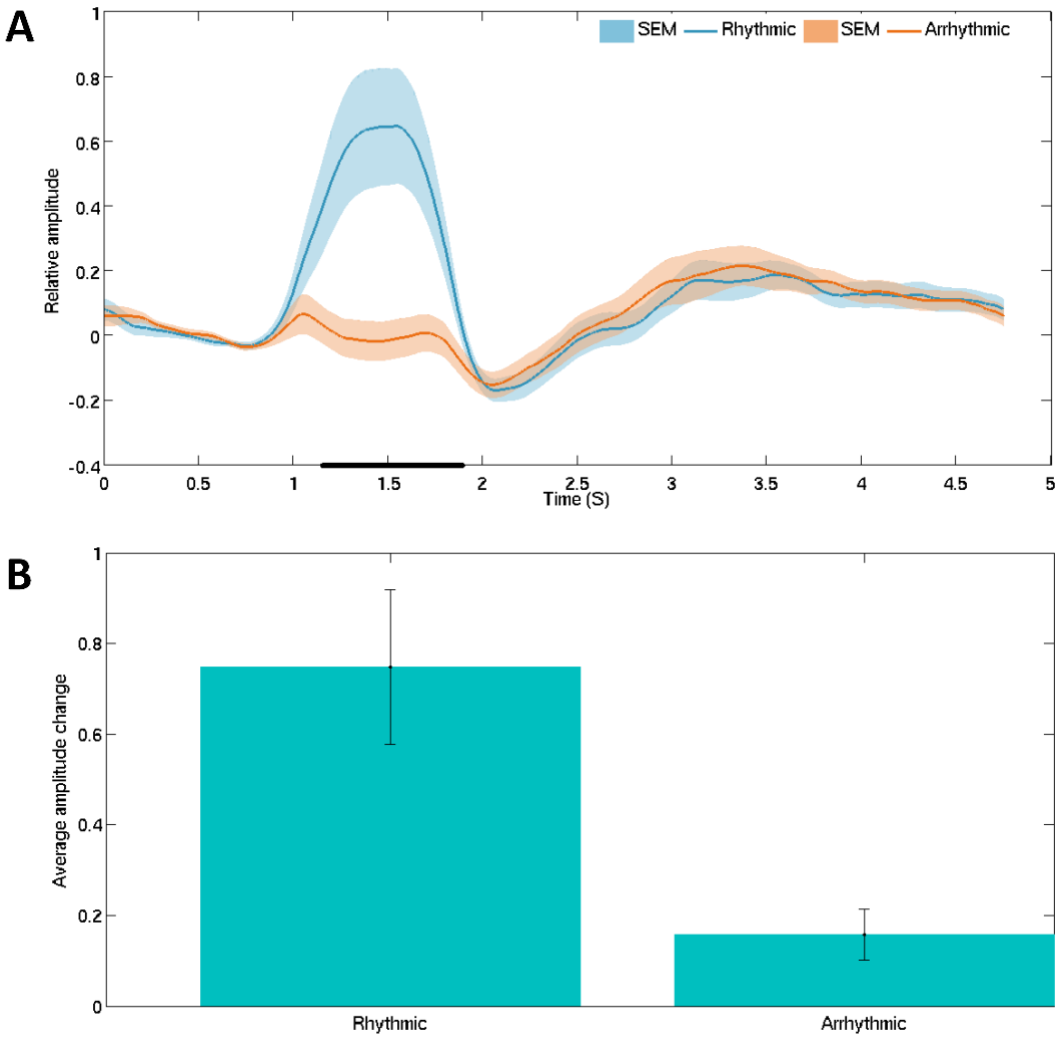

Figure 5. Comparison between rhythmic and arrhythmic 12Hz power changes.
A) A graph showing the difference in the 12Hz power in the rhythmic and arrhythmic conditions. A black line along the x-axis marks timepoints where a significant difference (p≤0.05) is seen (FDR corrected). B) A bar graph showing the average 12Hz power increase across trials during stimulation (p≤0.001).

1

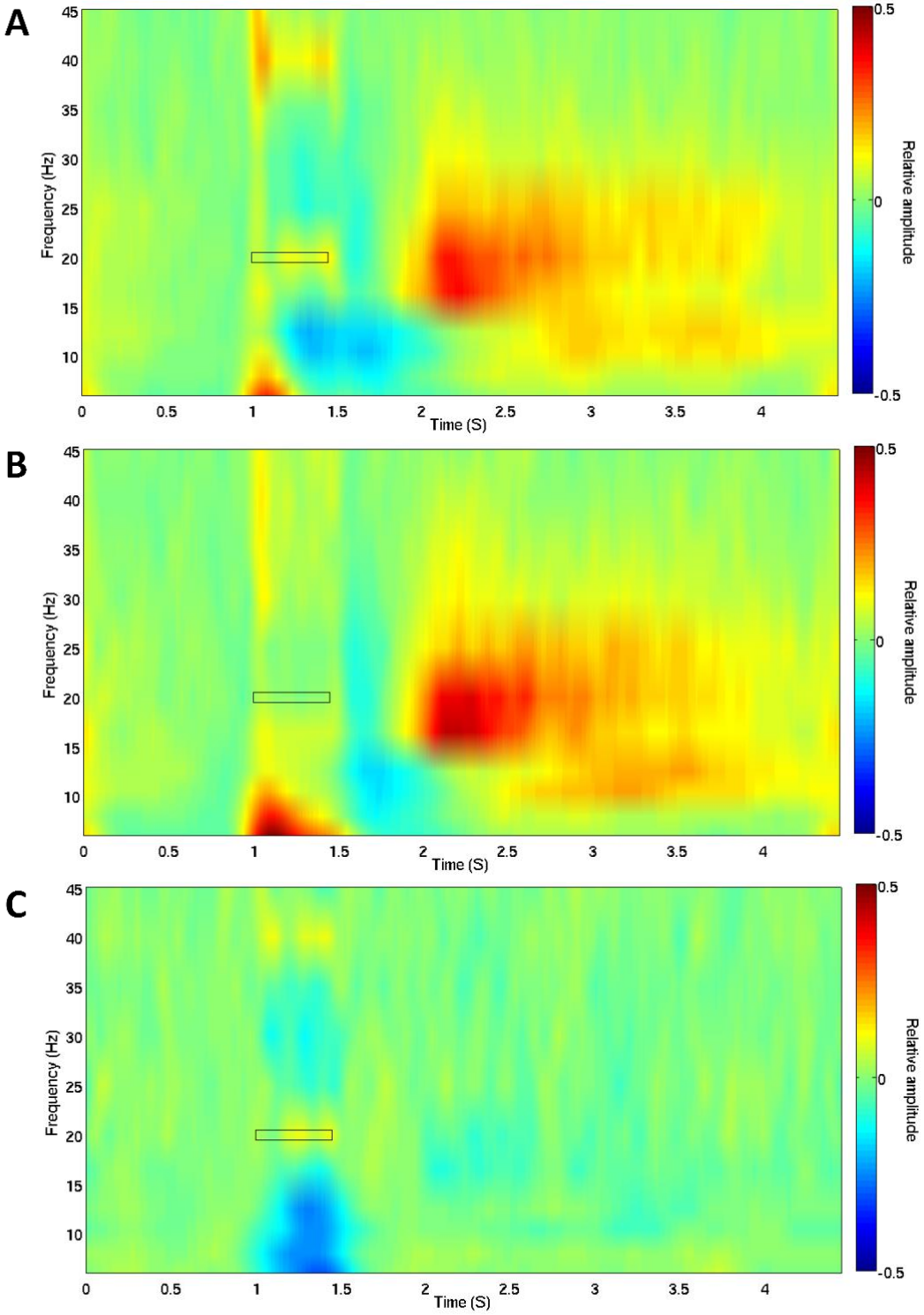

Figure 6. 20Hz power changes in the contralateral somatosensory cortex.
(A-C) TFSs of relative amplitude changes when 20Hz MNS was delivered between 1 and 1.45s in a A) rhythmic B) arrhythmic pattern with C) showing the difference in power between the two conditions.

1

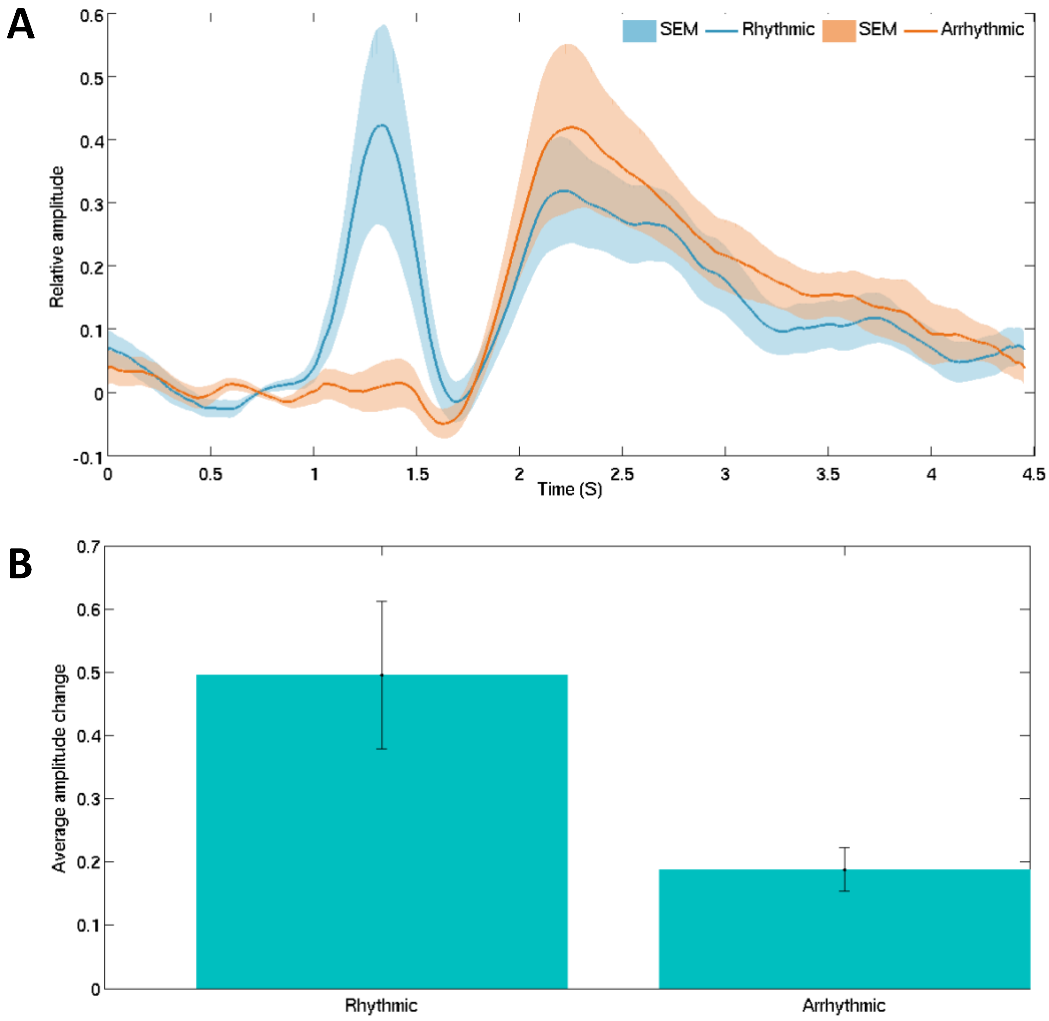

Figure 7. Comparison between rhythmic and arrhythmic 20Hz power changes.
A) A graph showing the difference in the relative 20Hz power in the rhythmic and arrhythmic conditions. B) A bar graph showing the average 20Hz power increase across trials during stimulation ($p < 0.01$).

3.2. Entrainment: Increase in Phase Coherence

For both rhythmic and arrhythmic stimulation, there was an initial increase in ITPC across a wide range of frequencies (Figure 8, Figure 9). After the first stimulation pulse, this increase in ITPC was maintained in only the rhythmic condition and centred on the frequency of stimulation and its harmonics (Figure 8A, Figure 9A). The ITPC within the window of stimulation was significantly higher in the rhythmic condition compared to arrhythmic (12Hz: $p \leq 0.05$ for 980-1995ms and 3303-3313ms, FDR corrected) (Figure 8D) (20Hz: $p < 0.05$ for 1083-1675ms, 3037-3042ms, 3045ms, 3047ms, 3065-3073ms and 4257-4292ms, FDR corrected) (Figure 9D).

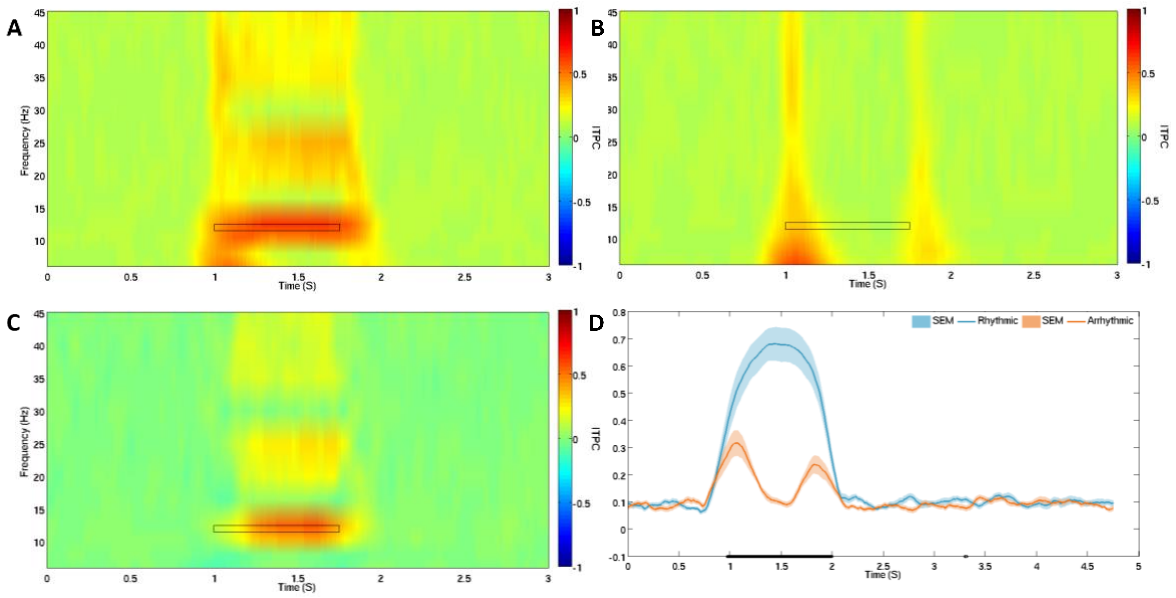

Figure 8. 12Hz inter-trial phase coherence in the contralateral somatosensory cortex.
TFSs of ITPC when 12Hz MNS was delivered between 1 and 1.75s in A) rhythmic B) arrhythmic pattern with C) showing the difference in phase coherence between the two conditions. D) A graph showing the difference in ITPC between the rhythmic and arrhythmic conditions. A black line along the x-axis marks timepoints where a significant difference ($p \leq 0.05$) is seen (FDR corrected).

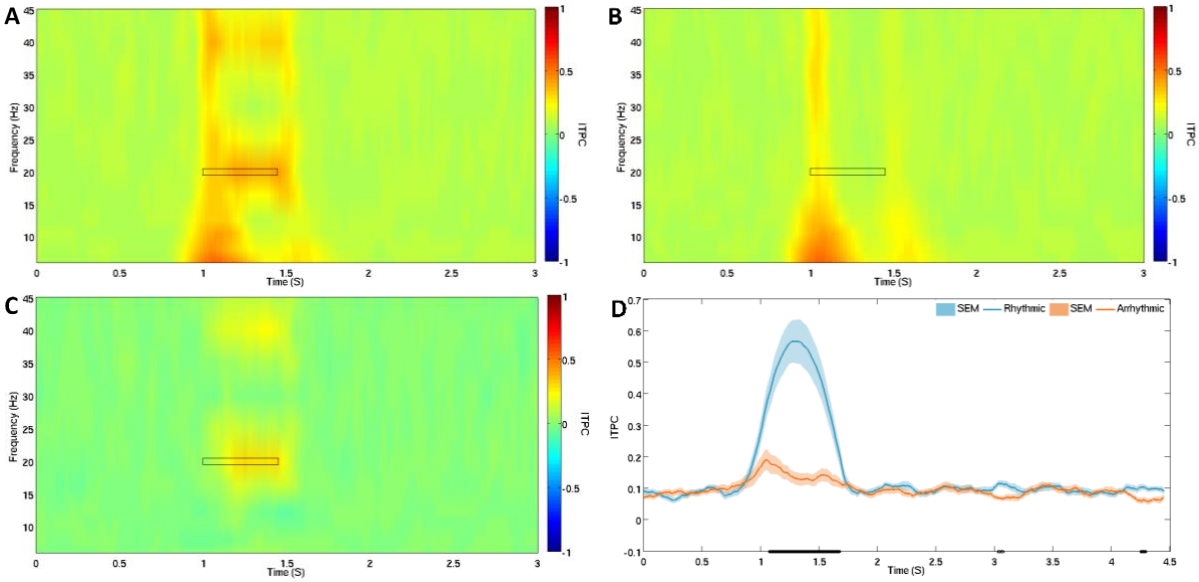

Figure 9. 20Hz inter-trial phase coherence in the contralateral somatosensory cortex.
(A-C) TFSs of ITPC when 20Hz MNS was delivered between 1 and 1.45s in a A) rhythmic B) arrhythmic pattern with C) showing the difference in phase coherence between the two conditions. D) A graph showing the difference between ITPC in the rhythmic and arrhythmic conditions.

3.3. Entrainment: Hemispheric Specificity

To investigate whether the effect was hemisphere specific, as suggested by the results shown in Figure 2 and Figure 3, we plotted the relative amplitude at the frequency of stimulation in the right and left somatosensory cortices during the rhythmic trials (Figure 10). The increase in power during the 12Hz rhythmic stimulation ($p \leq 0.05$ between 1147 and 1880ms, FDR corrected) and the subsequent rebound ($p \leq 0.05$ for 3485-3833ms, 3845ms, 4192-4263ms and 4518-4542ms, FDR corrected) were only seen in the left somatosensory cortex, which is contralateral to the stimulated arm. Conversely, the increase in power in the left versus the right hemisphere during the 20Hz rhythmic stimulation did not survive FDR correction. However, the subsequent rebound was only seen in the left somatosensory cortex as shown in Figure 11 where timepoints of statistical significance are indicated ($p < 0.05^{\text{FDR-corrected}}$).

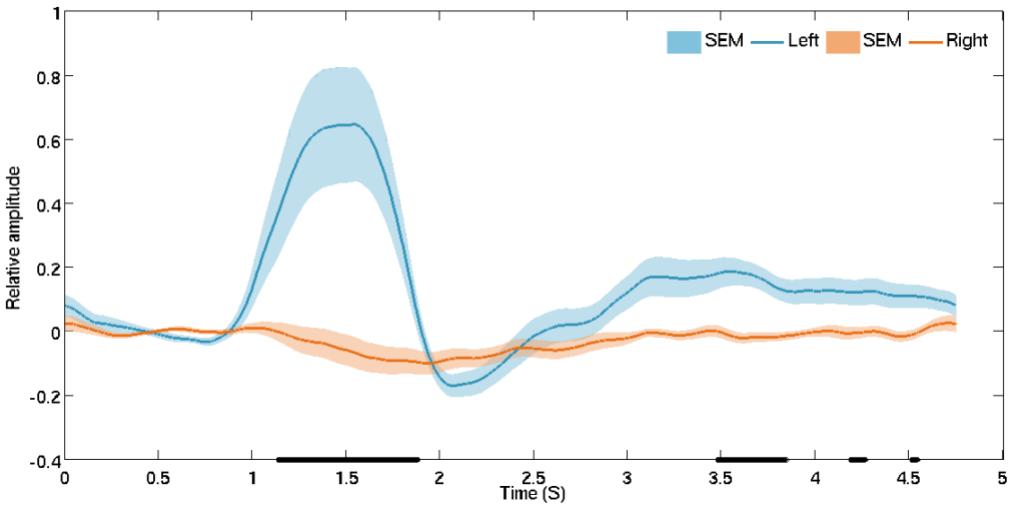

Figure 10. Hemispheric specificity of 12Hz entrainment.
A graph showing the difference in 12Hz power in the left (contralateral) and right (ipsilateral) hemisphere during 12Hz stimulation. A black line along the x-axis marks timepoints where a significant difference (p≤0.05) is seen (FDR corrected).

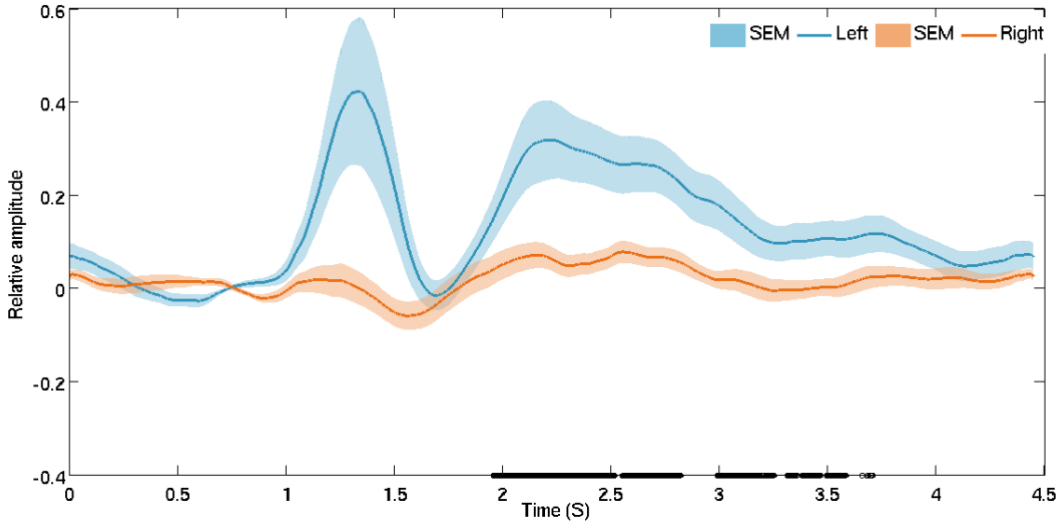

Figure 11. Hemispheric specificity of 20Hz entrainment.
A graph showing the difference in 20Hz power in the left (contralateral) and right (ipsilateral) hemisphere during 20Hz stimulation. A black line along the x-axis marks timepoints where a significant difference (p≤0.05) is seen (FDR corrected).

3.4. Sensory Evoked Potentials

A possible explanation for the increase in power and phase coherence seen during stimulation is that there was a SEP associated with each pulse of the MNS (Thut, Veniero, et al., 2011). To investigate whether this was the case, the raw oscillatory signal was filtered between 8-12Hz for the 12Hz stimulation trials and 13-30Hz for the 20Hz stimulation trials (Figure 12, Figure 13). Data from 2 participants was not included due to a loss of data, meaning we were unable to determine which trials were deleted during preprocessing, and as such could not determine the pulse timings for the remaining trials. Each subplot contains the data following the pulse timings in each condition for a complete oscillation at the frequency of stimulation meaning a timeframe of 83.3ms was used for the 12Hz trials and 50ms for the 20Hz trials. As is most evident in the 12Hz trials a full oscillatory cycle was associated with each pulse of both the rhythmic and arrhythmic trains. However, on investigation of the unfiltered data in the 12Hz trials, an evoked component was clearly associated with each pulse (Figure 14). Following the SEP evoked by the first pulse, the remainder of the evoked potentials appear to be smaller in amplitude. However, with the exception of the initial MNS pulse, the pulses of the 20Hz trials do not appear to be associated with a SEP (Figure 15). Furthermore, towards the end of the rhythmic stimulus train a full beta oscillation is seen with a significantly larger amplitude at the peaks compared to that of the arrhythmic data ($p < 0.05^{\text{FDR-corrected}}$). In Figure 12 and Figure 13 the timings were shifted by 20ms to account for the approximate time it would take for the afferent volley to reach the cortex. The data in Figure 14 and Figure 15 were not shifted and the negative deflection at ~20ms (N20 peak) reflects when the signal arrived in the primary somatosensory cortex (Passmore et al., 2014).

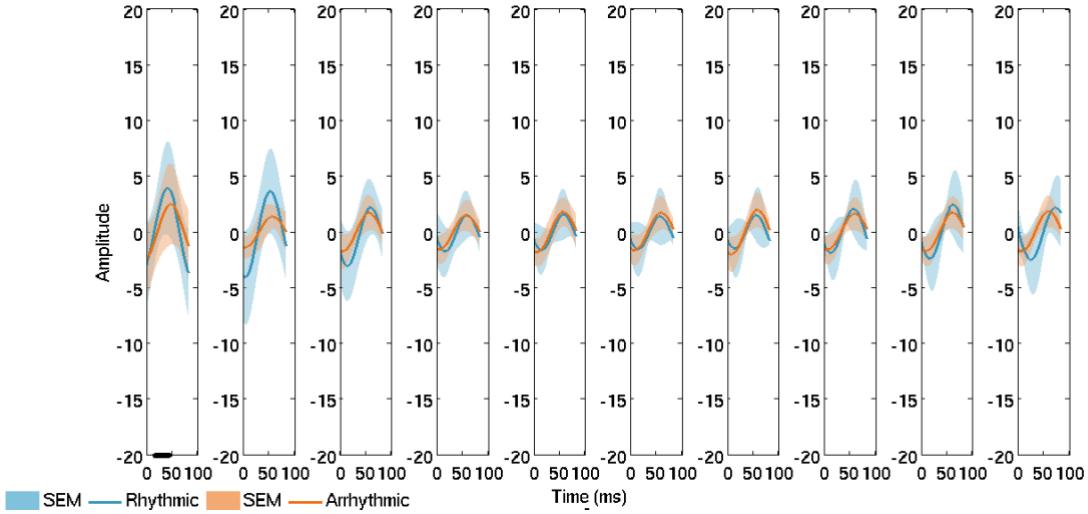

Figure 12. Mu band oscillatory response to each MNS pulse.
The 8-12Hz oscillatory response to each pulse of the rhythmic and arrhythmic 12Hz MNS.

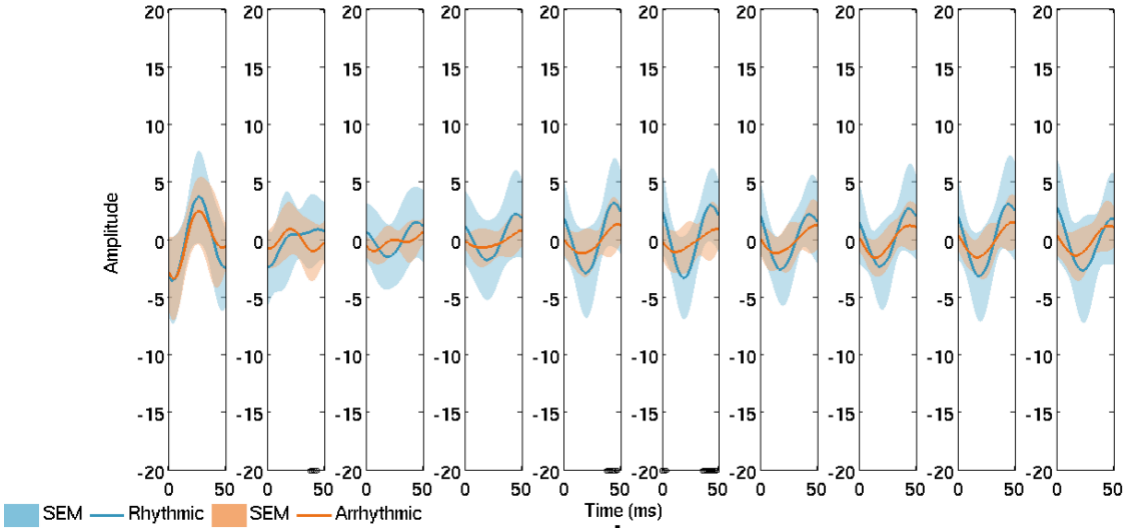

Figure 13. Beta band oscillatory response to each MNS pulse.
The 13-30Hz oscillatory response to each pulse of the rhythmic and arrhythmic 20Hz MNS.

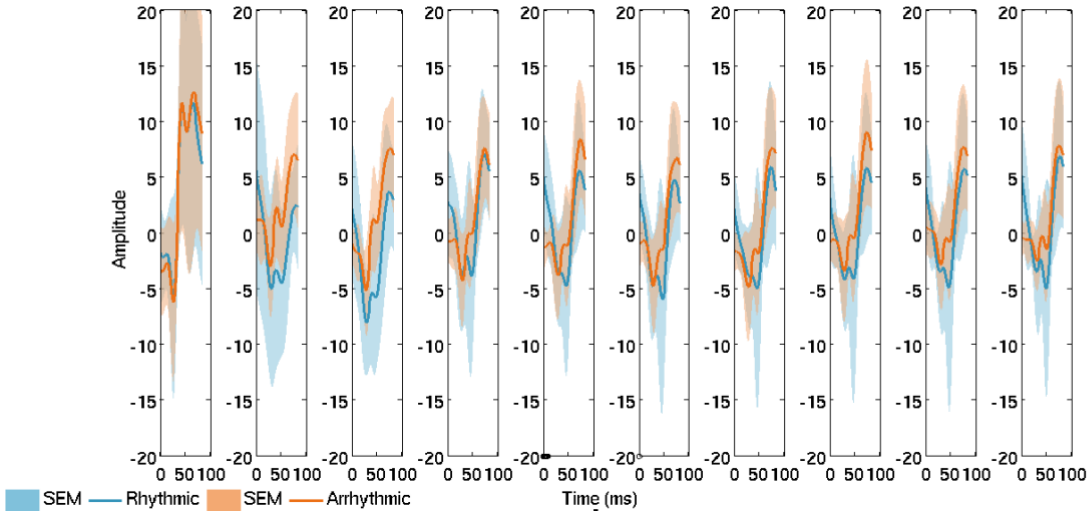

Figure 14. The unfiltered data from 12Hz trials.
A figure showing an evoked component associated with each pulse of the rhythmic and arrhythmic 12Hz MNS.

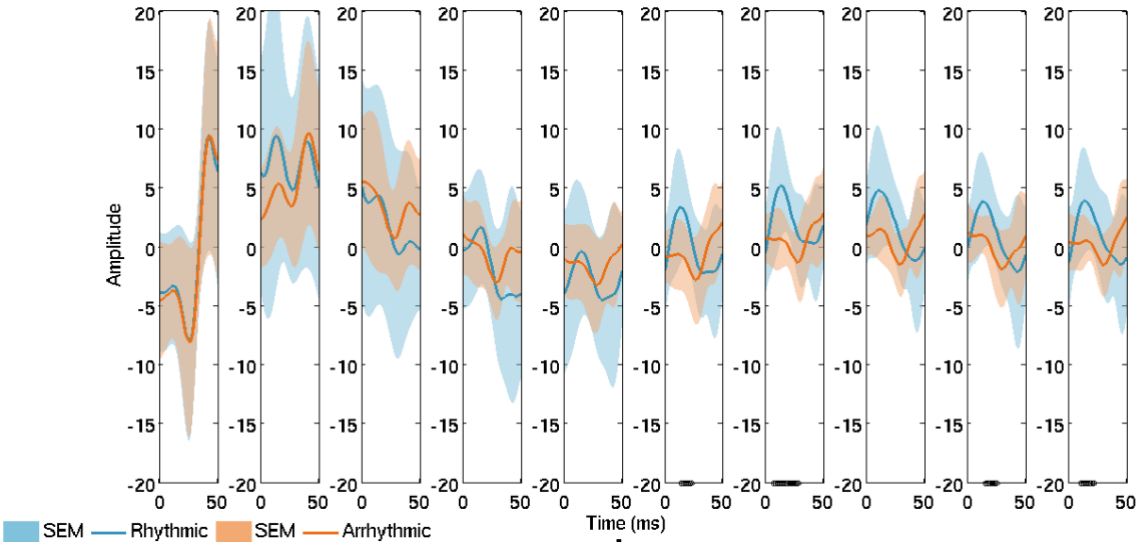

Figure 15. The unfiltered data from 20Hz trials.
A figure showing an evoked component associated with the first pulse of the rhythmic and arrhythmic 20Hz MNS and the progressive entrainment of beta oscillations in the rhythmic condition.

3.5. Post-hoc Analyses

Due to the evidence of aftereffects seen in the paper by Maiquez and colleagues (Morera Maiquez et al., 2020), we also investigated the broadband mu (8-12Hz) and beta (13-30Hz) effects following both 12Hz and 20Hz stimulation. The only significant effect was in the mu (8-12Hz) band during and for a short time following 20Hz arrhythmic stimulation compared to rhythmic stimulation, indicating a greater degree of suppression in the rhythmic trials ($p \leq 0.05$ at 1032-1532ms, FDR corrected) (Figure 16).

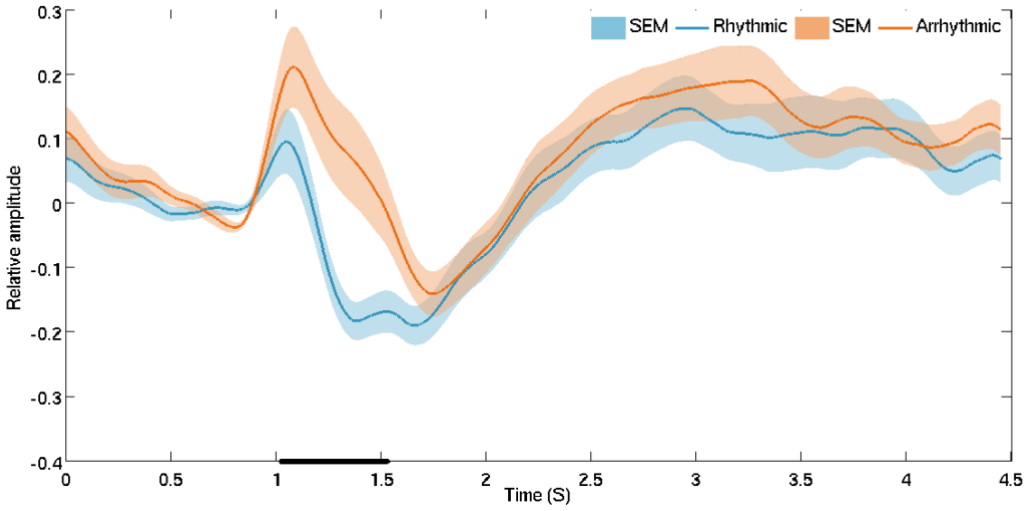

Figure 16. Mu-band aftereffects of 20Hz MNS.
A graph showing the difference in the relative 8-12Hz power when 20Hz MNS was delivered between 1 and 1.45s in a rhythmic or arrhythmic pattern. A black line along the x-axis marks timepoints where a significant difference ($p \leq 0.05$) is seen (FDR corrected).

As the beneficial effects of rhythmic MNS on tics is not restricted to the stimulated limb as demonstrated in a recent paper by Morera Maiquez and colleagues we decided to investigate the spread of the effect using a voxel LCMV beamformer **(Morera Maiquez et al., 2020)**. This revealed that the focus of the increase in power was in the contralateral sensorimotor hand region (

Appendix B).

4. Discussion

We investigated whether rhythmic MNS could be used to entrain oscillations at frequencies associated with sensorimotor inhibition, mu (12Hz) and beta (20Hz). Our results demonstrate that rhythmic 12Hz stimulation resulted in an increase in the relative amplitude and ITPC at 12Hz for the duration of the stimulation in the contralateral somatosensory cortex. Both of these findings can be split into two segments: 1) an increase in both power and coherence across a broad range of frequencies for the first pulse in both the rhythmic and arrhythmic trials; 2) an increase specific to the frequency of stimulation for the remainder of the pulse train, which was only seen in the rhythmic condition. However, we also show that for both rhythmic and arrhythmic 12Hz MNS, an evoked component was associated with each pulse of the stimulation. The effects on ITPC were replicated in the 20Hz condition, however the increase in relative amplitude and presence of evoked potentials was less clear. These results, and the evidence they provide as to whether MNS can entrain neuronal oscillations, are discussed below.

4.1. Steady-State Evoked Response

Thut et al., 2011 previously showed that ~10Hz TMS caused an initial broadband increase in power in both the rhythmic and arrhythmic stimulation conditions, before progressive entrainment was seen in the rhythmic condition (Thut, Veniero, et al., 2011). The authors proposed that the delivery of the first few pulses may have resulted in phase resetting of neural generators within the cortex whose frequencies of oscillation varied across a broad range of frequency bands (Thut, Veniero, et al., 2011). Therefore, phase resetting of these oscillators could have resulted in the initial broadband increase in power. The subsequent pulses however will have only occurred in phase with generators oscillating in the alpha band leading to progressive synchronisation of oscillations at this frequency (Thut, Veniero, et al., 2011).

Here we show that MNS causes an initial broadband increase in power, suggesting that peripheral stimulation triggers an initial phase reset of the neural generators within the contralateral somatosensory cortex regardless of the pattern of stimulation. In line with the theory of entrainment we see that the remainder of the rhythmic pulses cause a frequency specific increase in power. This is also mirrored in the ITPC results, where the initial broadband increase aligns with the theory that numerous neural generators phase reset resulting in phase coherence across trials. As the remaining rhythmic pulses are associated with an increased ITPC in the stimulated frequency band (and its harmonics) this shows that oscillations across trials are relatively more in phase during the stimulation suggesting synchronisation with the pulses of MNS.

However, one central issue in concluding that a rhythmic oscillatory response to a rhythmic stimulus is neural entrainment is whether the same data could be explained by rhythmic evoked potentials (For in-depth review please see (Thut, Schyns, et al., 2011; Zoefel et al., 2018)). If we deliver a stimulus at 12Hz it is expected that we would see a response 12 times a second (Zoefel et al., 2018). An investigation of this possibility by Capilla and colleagues showed that the oscillatory response seen during rhythmic stimulus presentation can be modelled through linear superposition of evoked potentials, which casts doubt on the explanation of entrainment (Capilla et al., 2011). Therefore, rhythmic SEPs mask at least in part any entrainment effect rhythmic MNS has on endogenous oscillations in the 12Hz condition. As both responses are expected to repeat at the same frequency, this makes it difficult to determine whether there is underlying entrainment (Zoefel et al., 2018). Furthermore, we would expect oscillations to continue after stimulation if entrainment had taken place (Thut, Schyns, et al., 2011; Zoefel et al., 2018). During entrainment oscillators become phase-aligned to the external source and, as phase is a free parameter, any change in phase alignment should only occur if the system is perturbed (Pikovskij et al., 2003). Here, we see a short-lived continuation of the increase in power after the last pulse of MNS, but this is could be due to the evoked potential associated with this last pulse.

In contrast to the 12Hz condition, the 20Hz rhythmic stimulation appears to show oscillations within the unfiltered data following the evoked potential associated with the first MNS pulse. Furthermore, towards the end of the stimulation train these oscillations have a higher amplitude, compared to those evoked by the arrhythmic stimulation suggesting that entrainment may have occurred. Previous experiments investigating steady-state responses of the somatosensory cortex have reported a maximal amplitude between 21 and 27 Hz (Muller et al., 2001; Snyder, 1992; Tobimatsu et al., 1999, 2000). In recent preprint, Walti and colleagues reported that somatosensory oscillations could be

entrained by vibrotactile stimulation at beta but not alpha frequency (Wälti et al., 2019). They concluded that their results could be explained by beta being the preferred frequency of the somatosensory system, a theory that our results also support (Wälti et al., 2019).

Nevertheless, the evoked potentials and entrained oscillations are generated by synchronous firing of neuronal populations within the contralateral somatosensory cortex meaning these neurons are 'occupied' in processing of the afferent input. It is thought that there is a high level of 'sensorimotor noise' associated with the occurrence of tics in TS leading to a difficulty in discriminating between the signals preceding voluntary and involuntary movement (Ganos et al., 2015). Increasing synchronised firing of neuronal populations within the sensorimotor cortex through MNS may lead to a decrease in this noise. Alternatively, it is known that ~20ms following median nerve stimulation there is a decrease in the amplitude of MEPs elicited by a TMS pulse to the contralateral motor cortex in a process known as short afferent inhibition (SAI) (Tokimura et al., 2000). As there is thought to be a deficit in this form of inhibition in TS patients it could be that continuous MNS compensates for this deficit and aids in the inhibition of tics and urges (Morera Maiquez et al., 2020; Orth et al., 2005; Orth & Rothwell, 2009). Considering 12Hz arrhythmic stimulation also elicits an evoked potential in the sensory cortex it is therefore of interest as to whether arrhythmic stimulation also reduces the frequency of tics i.e. is the beneficial effect due to SAI and/or a decrease in sensorimotor noise, or is the rhythmicity of the stimulation important (Morera Maiquez et al., 2020).

4.2. Aftereffects of Rhythmic Stimulation

The observance of a desynchronisation and rebound following MNS trains is typical of that seen following one pulse of MNS (Pfurtscheller, 1981). The only significant difference in the aftereffect seen here was greater desynchronization in the 8-12Hz band following 20Hz rhythmic stimulation compared to arrhythmic. This contrasts with recent findings which indicated that there was greater mu and beta desynchronization and increased beta rebound following 19Hz arrhythmic stimulation (Maiquez et al., 2020)(preprint). On inspection of the data reported by Maiquez and colleagues, there is a short period of increased mu suppression during and following rhythmic stimulation as seen in our data. This suggests that the typical mu band desynchronization seen during movement is maintained in the rhythmic condition. However, further findings by the same authors also describe greater beta desynchronization and increased beta rebound following 12Hz arrhythmic stimulation (Morera Maiquez et al., 2020). We hypothesise that these differences in beta aftereffects may have arisen due to a combination of several factors. Firstly study design, our experiment along with the two previous studies left only 4 seconds between each trial during which the post-movement beta rebound may be

still ongoing (Pakenham et al., 2020), critically this is also the period during which the experiments defined their control windows. This means that the baseline was likely contaminated by higher beta power, the extent to which likely depended on both the sample group and the condition of the preceding trial, which in the current study could have been either 12 or 20Hz. Investigation of the uncorrected TFS confirms a high level of beta power continues throughout the control window. Secondly, the subjective nature of the visible thumb twitch may have led to participants in one study experiencing higher intensities of stimulation. Therefore, future investigations into the effects of rhythmic MNS should ideally use longer intertrial intervals to allow for beta rebound (Pakenham et al., 2020), and an objective method of thresholding, for example, through measurement of MEPs as is common practice with TMS. The need to standardise motor thresholding for MNS becomes apparent with the large variation in baseline MEP amplitude despite intensity thresholding being completed by the same experimenter each time.

4.3. Conclusion

Ultimately, the evidence from this research suggests that endogenous oscillations within the somatosensory cortex can be entrained by 20Hz rhythmic MNS. On the other hand, the oscillatory effects of 12Hz rhythmic MNS are largely caused by the presence of rhythmic SEPs. As SEPs are present in both the rhythmic and arrhythmic 12Hz conditions, investigation of the effect of arrhythmic stimulation on tics and urges is warranted. Nonetheless, the behavioural effects of rhythmic peripheral nerve stimulation are clinically important, however a better understanding of how these behavioural effects are produced is vital for fine-tuning their development as a therapeutic technique (Morera Maiquez et al., 2020).

Author Contributions

MH. Conceptualisation, Experimental design, Data analysis, Data interpretation, Writing paper - Original Draft.

BM. Conceptualisation, Experimental design, Data interpretation, Writing paper – Review and Editing.

MB. Data analysis, Data interpretation, Writing paper – Review and Editing.

SJ. Conceptualisation, Experimental design, Data interpretation, Writing paper – Review and Editing.

Declaration of Conflicting Interests

None

Acknowledgments

Data collection for this paper was supported by research grant from NIHR Nottingham Biomedical Research Centre. The views expressed are those of the authors and not necessarily those of the NHS, the NIHR or the Department of Health.

References

Asamoah, B., Khatoun, A., & Mc Laughlin, M. (2019). TACS motor system effects can be caused by transcutaneous stimulation of peripheral nerves. *Nature Communications*, *10*(1), 266. https://doi.org/10.1038/s41467-018-08183-w

Benjamini, Y., & Hochberg, Y. (1995). Controlling the False Discovery Rate: A Practical and Powerful Approach to Multiple Testing. *Journal of the Royal Statistical Society: Series B (Methodological)*, *57*(1), 289–300. https://doi.org/10.1111/j.2517-6161.1995.tb02031.x

Benjamini, Y., & Yekutieli, D. (2001). The control of the false discovery rate in multiple testing under dependency. *The Annals of Statistics*, *29*(4), 1165–1188.

Brinkman, L., Stolk, A., Marshall, T. R., Esterer, S., Sharp, P., Dijkerman, H. C., de Lange, F. P., & Toni, I. (2016). Independent Causal Contributions of Alpha- and Beta-Band Oscillations during Movement Selection. *The Journal of Neuroscience*, *36*(33), 8726–8733. https://doi.org/10.1523/JNEUROSCI.0868-16.2016

Brookes, M. J., Vrba, J., Robinson, S. E., Stevenson, C. M., Peters, A. M., Barnes, G. R., Hillebrand, A., & Morris, P. G. (2008). Optimising experimental design for MEG beamformer imaging. *NeuroImage*, *39*(4), 1788–1802. https://doi.org/10.1016/j.neuroimage.2007.09.050

Capilla, A., Pazo-Alvarez, P., Darriba, A., Campo, P., & Gross, J. (2011). Steady-State Visual Evoked Potentials Can Be Explained by Temporal Superposition of Transient Event-Related Responses. *PLoS ONE*, *6*(1), e14543. https://doi.org/10.1371/journal.pone.0014543

Chen, R., Yaseen, Z., Cohen, L. G., & Hallett, M. (1998). Time course of corticospinal excitability in reaction time and self-paced movements. *Annals of Neurology*, *44*(3), 317–325. https://doi.org/10.1002/ana.410440306

Cheyne, D. O. (2013). MEG studies of sensorimotor rhythms: A review. *Experimental Neurology*, *245*, 27–39. https://doi.org/10.1016/j.expneurol.2012.08.030

Colclough, G. L., Brookes, M. J., Smith, S. M., & Woolrich, M. W. (2015). A symmetric multivariate leakage correction for MEG connectomes. *NeuroImage*, *117*, 439–448. https://doi.org/10.1016/j.neuroimage.2015.03.071

Colon, E., Legrain, V., & Mouraux, A. (2012). Steady-state evoked potentials to study the processing of tactile and nociceptive somatosensory input in the human brain. *Neurophysiologie Clinique/Clinical Neurophysiology*, *42*(5), 315–323. https://doi.org/10.1016/j.neucli.2012.05.005

Engel, A. K., & Fries, P. (2010). Beta-band oscillations—Signalling the status quo? *Current Opinion in Neurobiology*, *20*(2), 156–165. https://doi.org/10.1016/j.conb.2010.02.015

Ganos, C., Asmuss, L., Bongert, J., Brandt, V., Münchau, A., & Haggard, P. (2015). Volitional action as perceptual detection: Predictors of conscious intention in adolescents with tic disorders. *Cortex*, *64*, 47–54. https://doi.org/10.1016/j.cortex.2014.09.016

Gilbertson, T. (2005). Existing Motor State Is Favored at the Expense of New Movement during 13-35 Hz Oscillatory Synchrony in the Human Corticospinal System. *Journal of Neuroscience*, *25*(34), 7771–7779. https://doi.org/10.1523/JNEUROSCI.1762-05.2005

Gong, G., He, Y., Concha, L., Lebel, C., Gross, D. W., Evans, A. C., & Beaulieu, C. (2009). Mapping Anatomical Connectivity Patterns of Human Cerebral Cortex Using In Vivo Diffusion Tensor Imaging Tractography. *Cerebral Cortex*, *19*(3), 524–536. https://doi.org/10.1093/cercor/bhn102

Groppe, D. (2020). *Fdr_bh*. MATLAB Central File Exchange. https://uk.mathworks.com/matlabcentral/fileexchange/27418-fdr_bh

Haegens, S., Osipova, D., Oostenveld, R., & Jensen, O. (2009). Somatosensory working memory performance in humans depends on both engagement and disengagement of regions in a distributed network. *Human Brain Mapping*, NA-NA. https://doi.org/10.1002/hbm.20842

Herrmann, C. S. (2001). Human EEG responses to 1-100 Hz flicker: Resonance phenomena in visual cortex and their potential correlation to cognitive phenomena. *Experimental Brain Research*, *137*(3–4), 346–353. https://doi.org/10.1007/s002210100682

Huang, M. X., Mosher, J. C., & Leahy, R. M. (1999). A sensor-weighted overlapping-sphere head model and exhaustive head model comparison for MEG. *Physics in Medicine and Biology*, *44*(2), 423–440. https://doi.org/10.1088/0031-9155/44/2/010

Jenkinson, M., Beckmann, C. F., Behrens, T. E. J., Woolrich, M. W., & Smith, S. M. (2012). FSL. *NeuroImage*, *62*(2), 782–790. https://doi.org/10.1016/j.neuroimage.2011.09.015

Jenkinson, N., & Brown, P. (2011). New insights into the relationship between dopamine, beta oscillations and motor function. *Trends in Neurosciences*, *34*(12), 611–618. https://doi.org/10.1016/j.tins.2011.09.003

Jensen, O., & Mazaheri, A. (2010). Shaping Functional Architecture by Oscillatory Alpha Activity: Gating by Inhibition. *Frontiers in Human Neuroscience*, *4*. https://doi.org/10.3389/fnhum.2010.00186

Jurkiewicz, M. T., Gaetz, W. C., Bostan, A. C., & Cheyne, D. (2006). Post-movement beta rebound is generated in motor cortex: Evidence from neuromagnetic recordings. *NeuroImage*, *32*(3), 1281–1289. https://doi.org/10.1016/j.neuroimage.2006.06.005

Keitel, C., Quigley, C., & Ruhnau, P. (2014). Stimulus-Driven Brain Oscillations in the Alpha Range: Entrainment of Intrinsic Rhythms or Frequency-Following Response? *Journal of Neuroscience*, *34*(31), 10137–10140. https://doi.org/10.1523/JNEUROSCI.1904-14.2014

Maiquez, B. M., Jackson, G. M., & Jackson, S. R. (2020). *Entraining movement-related brain oscillations using rhythmic median nerve stimulation* [Preprint]. Neuroscience. https://doi.org/10.1101/2020.03.30.016097

Martínez-Cagigal, V. (2020). *Shaded area error plot*. MATLAB Central File Exchange. https://uk.mathworks.com/matlabcentral/fileexchange/58262-shaded-area-error-bar-plot

Morera Maiquez, B., Sigurdsson, H. P., Dyke, K., Clarke, E., McGrath, P., Pasche, M., Rajendran, A., Jackson, G. M., & Jackson, S. R. (2020). Entraining Movement-Related Brain Oscillations to Suppress Tics in Tourette Syndrome (in press). *Current Biology*, S0960982220305583. https://doi.org/10.1016/j.cub.2020.04.044

Muller, G. R., Neuper, Ch., & Pfurtscheller, G. (2001). „Resonance-like“ Frequencies of Sensorimotor Areas Evoked by Repetitive Tactile Stimulation—Resonanzeffekte in sensomotorischen Arealen, evoziert durch rhythmische taktile Stimulation. *Biomedizinische Technik/Biomedical Engineering*, *46*(7–8), 186–190. https://doi.org/10.1515/bmte.2001.46.7-8.186

Muthukumaraswamy, S. D. (2014). The use of magnetoencephalography in the study of psychopharmacology (pharmaco-MEG). *Journal of Psychopharmacology*, *28*(9), 815–829. https://doi.org/10.1177/0269881114536790

Notbohm, A., Kurths, J., & Herrmann, C. S. (2016). Modification of Brain Oscillations via Rhythmic Light Stimulation Provides Evidence for Entrainment but Not for Superposition of Event-Related Responses. *Frontiers in Human Neuroscience*, *10*. https://doi.org/10.3389/fnhum.2016.00010

Oldfield, R. C. (1971). The assessment and analysis of handedness: The Edinburgh inventory. *Neuropsychologia*, *9*(1), 97–113. https://doi.org/10.1016/0028-3932(71)90067-4

O'Neill, G. C., Tewarie, P. K., Colclough, G. L., Gascoyne, L. E., Hunt, B. A. E., Morris, P. G., Woolrich, M. W., & Brookes, M. J. (2017). Measurement of dynamic task related functional networks using MEG. *NeuroImage*, *146*, 667–678. https://doi.org/10.1016/j.neuroimage.2016.08.061

Orth, M., Amann, B., Robertson, M. M., & Rothwell, J. C. (2005). Excitability of motor cortex inhibitory circuits in Tourette syndrome before and after single dose nicotine. *Brain*, *128*(6), 1292–1300. https://doi.org/10.1093/brain/awh473

Orth, M., & Rothwell, J. C. (2009). Motor cortex excitability and comorbidity in Gilles de la Tourette syndrome. *Journal of Neurology, Neurosurgery & Psychiatry*, *80*(1), 29–34. https://doi.org/10.1136/jnnp.2008.149484

Pakenham, D. O., Quinn, A. J., Fry, A., Francis, S. T., Woolrich, M. W., Brookes, M. J., & Mullinger, K. J. (2020). Post-stimulus beta responses are modulated by task duration. *NeuroImage*, *206*, 116288. https://doi.org/10.1016/j.neuroimage.2019.116288

Passmore, S. R., Murphy, B., & Lee, T. D. (2014). The origin, and application of somatosensory evoked potentials as a neurophysiological technique to investigate neuroplasticity. *The Journal of the Canadian Chiropractic Association*, *58*(2), 170–183.

Pfurtscheller, G. (1981). Central beta rhythm during sensorimotor activities in man. *Electroencephalography and Clinical Neurophysiology*, *51*(3), 253–264. https://doi.org/10.1016/0013-4694(81)90139-5

Pfurtscheller, G., Stancák, A., & Neuper, C. (1996). Post-movement beta synchronization. A correlate of an idling motor area? *Electroencephalography and Clinical Neurophysiology*, *98*(4), 281–293. https://doi.org/10.1016/0013-4694(95)00258-8

Pikovskij, A., Rosenblum, M., & Kurths, J. (2003). *Synchronization: A universal concept in nonlinear sciences* (1st paperback ed., repr). Cambridge Univ. Press.

Pogosyan, A., Gaynor, L. D., Eusebio, A., & Brown, P. (2009). Boosting Cortical Activity at Beta-Band Frequencies Slows Movement in Humans. *Current Biology*, *19*(19), 1637–1641. https://doi.org/10.1016/j.cub.2009.07.074

Regan, D. (1966). Some characteristics of average steady-state and transient responses evoked by modulated light. *Electroencephalography and Clinical Neurophysiology*, *20*(3), 238–248. https://doi.org/10.1016/0013-4694(66)90088-5

Sarvas, J. (1987). Basic mathematical and electromagnetic concepts of the biomagnetic inverse problem. *Physics in Medicine and Biology*, *32*(1), 11–22.

Snyder, A. Z. (1992). Steady-state vibration evoked potentials: Description of technique and characterization of responses. *Electroencephalography and Clinical Neurophysiology/Evoked Potentials Section*, *84*(3), 257–268. https://doi.org/10.1016/0168-5597(92)90007-X

Thut, G., Schyns, P. G., & Gross, J. (2011). Entrainment of Perceptually Relevant Brain Oscillations by Non-Invasive Rhythmic Stimulation of the Human Brain. *Frontiers in Psychology*, *2*. https://doi.org/10.3389/fpsyg.2011.00170

Thut, G., Veniero, D., Romei, V., Miniussi, C., Schyns, P., & Gross, J. (2011). Rhythmic TMS Causes Local Entrainment of Natural Oscillatory Signatures. *Current Biology*, *21*(14), 1176–1185. https://doi.org/10.1016/j.cub.2011.05.049

Tobimatsu, S., Zhang, Y. M., & Kato, M. (1999). Steady-state vibration somatosensory evoked potentials: Physiological characteristics and tuning function. *Clinical Neurophysiology*, *110*(11), 1953–1958. https://doi.org/10.1016/S1388-2457(99)00146-7

Tobimatsu, S., Zhang, Y. M., Suga, R., & Kato, M. (2000). Differential temporal coding of the vibratory sense in the hand and foot in man. *Clinical Neurophysiology*, *111*(3), 398–404. https://doi.org/10.1016/S1388-2457(99)00278-3

Tokimura, H., Di Lazzaro, V., Tokimura, Y., Oliviero, A., Profice, P., Insola, A., Mazzone, P., Tonali, P., & Rothwell, J. C. (2000). Short latency inhibition of human hand motor cortex by somatosensory input from the hand. *The Journal of Physiology*, *523 Pt 2*, 503–513.

Tzourio-Mazoyer, N., Landeau, B., Papathanassiou, D., Crivello, F., Etard, O., Delcroix, N., Mazoyer, B., & Joliot, M. (2002). Automated Anatomical Labeling of Activations in SPM Using a Macroscopic

Anatomical Parcellation of the MNI MRI Single-Subject Brain. *NeuroImage*, *15*(1), 273–289. https://doi.org/10.1006/nimg.2001.0978

Van Veen, B. D., Van Drongelen, W., Yuchtman, M., & Suzuki, A. (1997). Localization of brain electrical activity via linearly constrained minimum variance spatial filtering. *IEEE Transactions on Biomedical Engineering*, *44*(9), 867–880. https://doi.org/10.1109/10.623056

Vialatte, F.-B., Maurice, M., Dauwels, J., & Cichocki, A. (2010). Steady-state visually evoked potentials: Focus on essential paradigms and future perspectives. *Progress in Neurobiology*, *90*(4), 418–438. https://doi.org/10.1016/j.pneurobio.2009.11.005

Wälti, M. J., Bächinger, M., Ruddy, K. L., & Wenderoth, N. (2019). *Steady-state responses in the somatosensory system interact with endogenous beta activity* [Preprint]. Neuroscience. https://doi.org/10.1101/690495

Zoefel, B., ten Oever, S., & Sack, A. T. (2018). The Involvement of Endogenous Neural Oscillations in the Processing of Rhythmic Input: More Than a Regular Repetition of Evoked Neural Responses. *Frontiers in Neuroscience*, *12*, 95. https://doi.org/10.3389/fnins.2018.00095

Appendix A

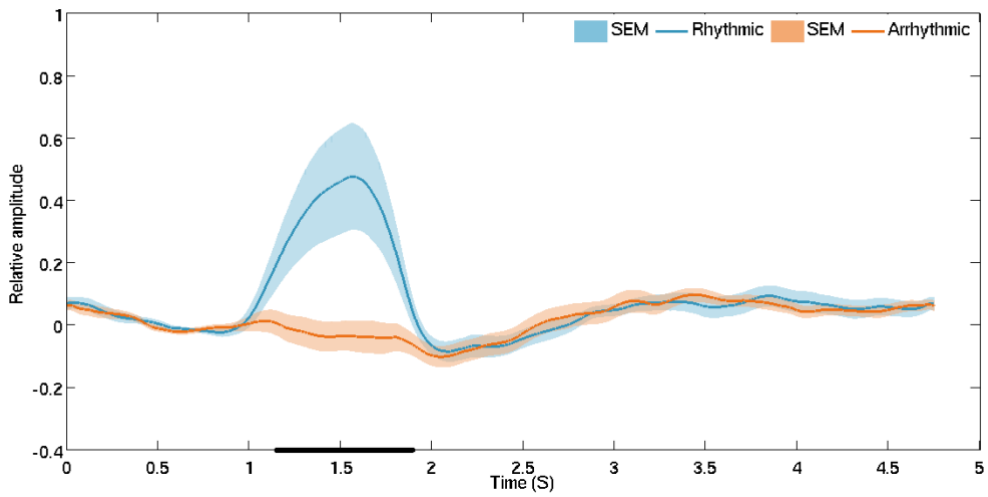

Figure A.1. Comparison between rhythmic and arrhythmic 12Hz power changes in the contralateral motor cortex.

A graph showing the difference in the relative 12Hz power in the rhythmic and arrhythmic conditions.

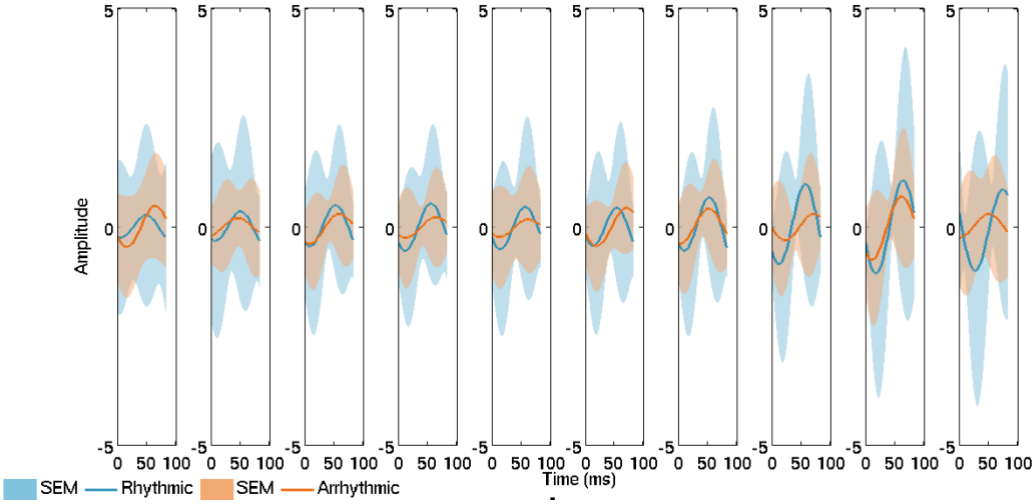

Figure A.3. Mu band oscillatory response in the contralateral motor cortex to each MNS pulse.
The 8-12Hz oscillatory response to each pulse of the rhythmic and arrhythmic 12Hz MNS.

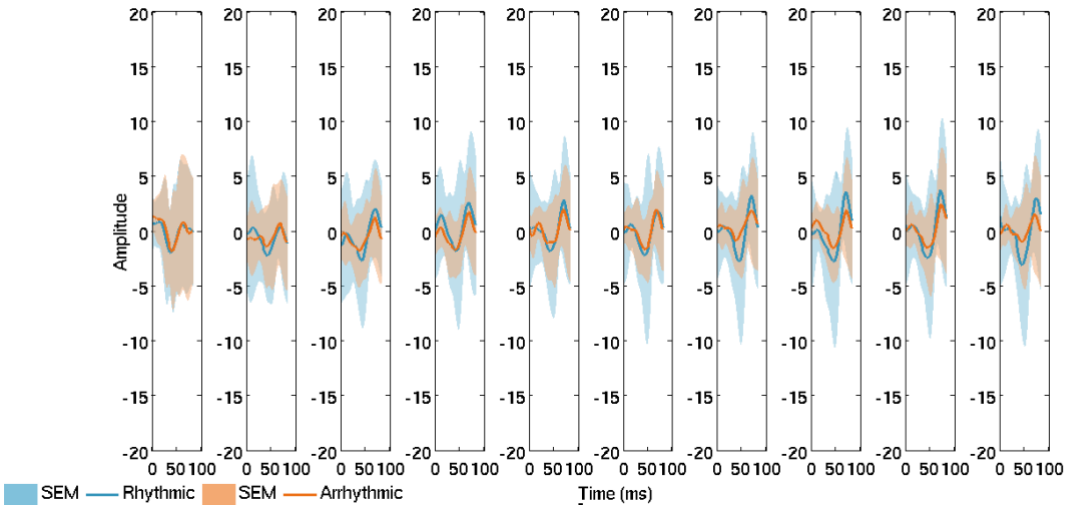

Figure A.4. The unfiltered data from the contralateral motor cortex.
A figure showing an evoked component associated with each pulse of the rhythmic and arrhythmic 12Hz MNS.

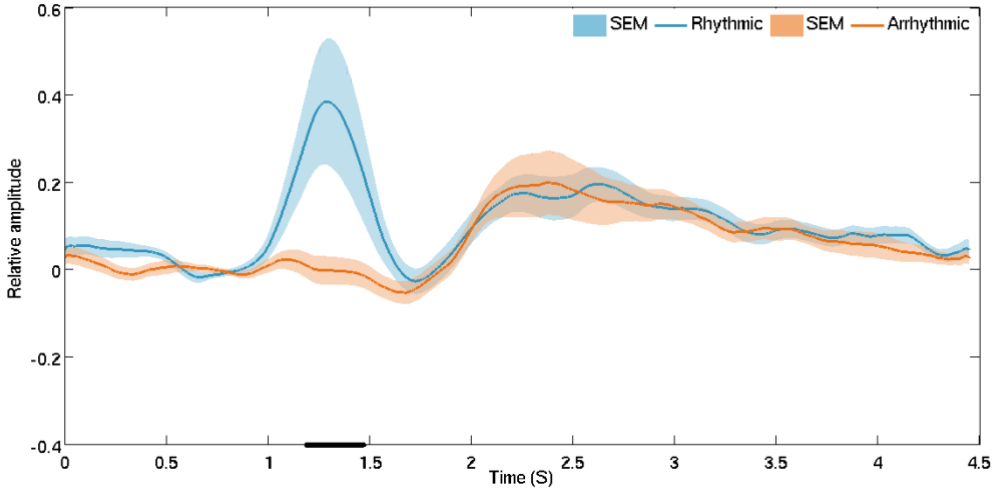

Figure A.5. Comparison between rhythmic and arrhythmic 20Hz power changes in the contralateral motor cortex.

A graph showing the difference in the relative 20Hz power in the rhythmic and arrhythmic conditions.

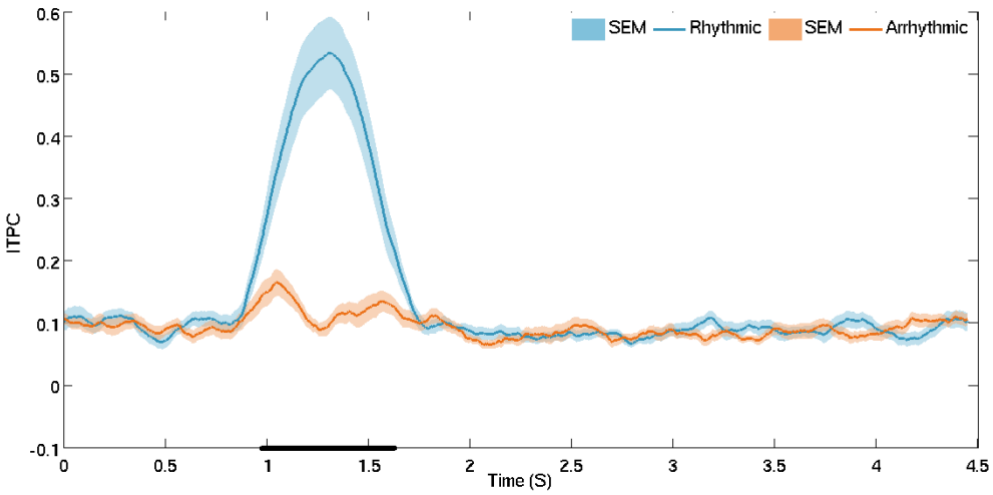

Figure A.6. 20Hz inter-trial phase coherence in the contralateral motor cortex.
A graph showing the difference between ITPC in the rhythmic and arrhythmic conditions.

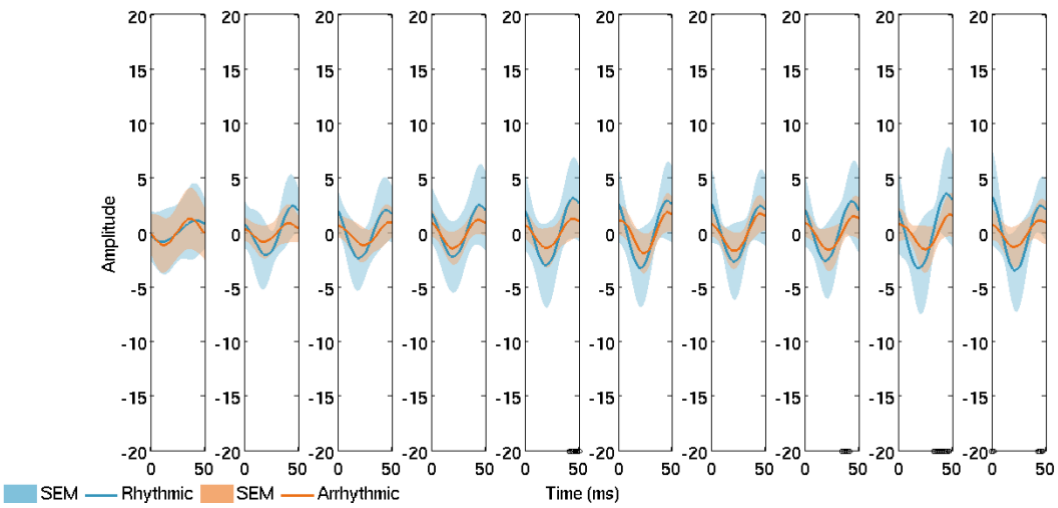

Figure A.7. Beta band oscillatory response in the contralateral motor cortex to each MNS pulse.
The 13-30Hz oscillatory response to each pulse of the rhythmic and arrhythmic 20Hz MNS.

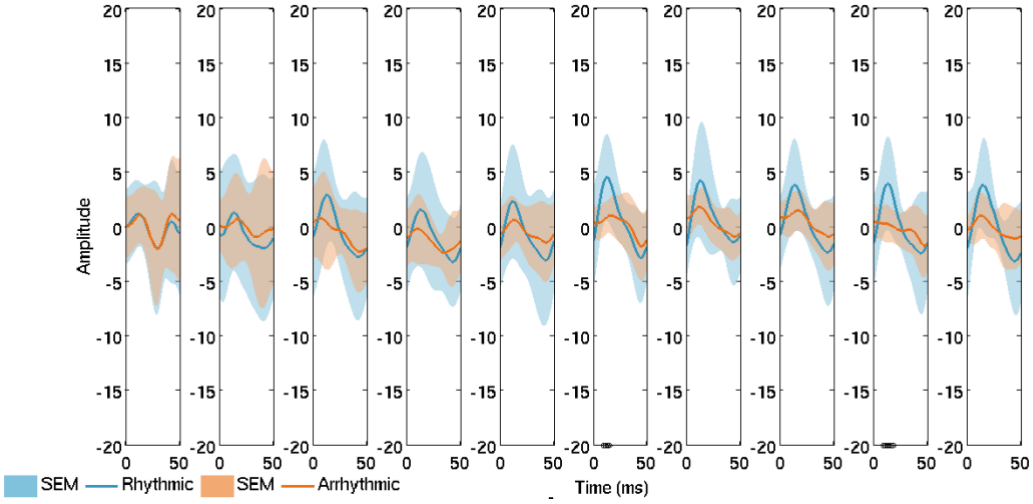

Figure A.8. The unfiltered data from the contralateral motor cortex.
A figure showing the progressive entrainment of beta oscillations in the rhythmic 20Hz condition.

Appendix B

A LCMV beamformer was applied to the preprocessed data to allow comparison of the data in the active (20Hz [1s 1.45s]; 12Hz [1s 1.75s]) and passive (20Hz [0.54s 0.99s]; 12Hz [0.24s 0.99s]) windows, for rhythmic MNS at the frequency of stimulation. Beamformer weights were calculated for each voxel, to create a pseudo-T-statistic map for each condition. Covariance was calculated for the entire experimental time window in a frequency window set according to the frequency of stimulation (19-21Hz and 11-13Hz). The covariance matrix of the filtered data was regularised using the Tikhonov method, with the regularisation parameter set at 4% of the maximum singular value. Individual maps were sampled on a 4mm grid of the subject's anatomical scan. For the group average (Figure), individual maps were subsequently transformed to MNI coordinate space using FLIRT. The neural generator of the entrained oscillations was identified using the peak amplitude in the frequency band of interest on the pseudo-T-statistic map.

1

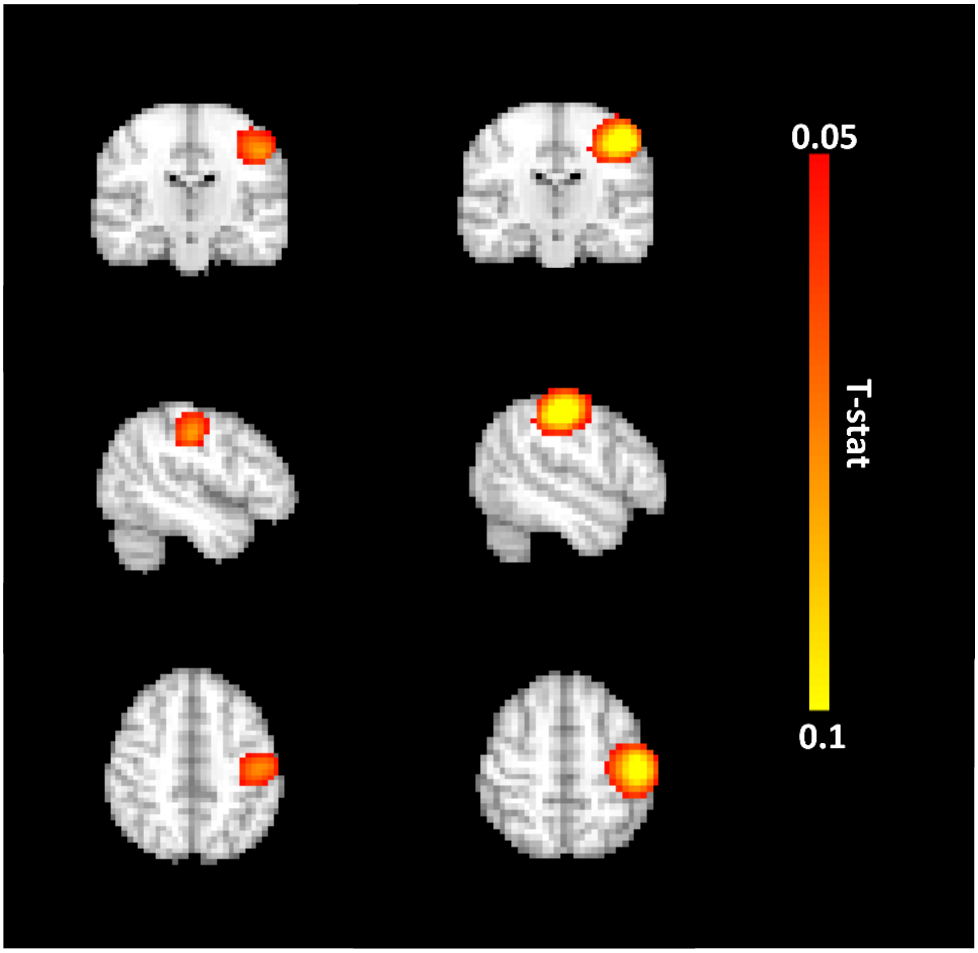

Figure B.1. Pseudo-t-statistical map

A figure showing the average location of the power increase during rhythmic stimulation at 12 (right) and 20Hz (left) localises to the contralateral sensorimotor hand region (MNI space) (radiological orientation).